Journal of
Synchrotron
Radiation

ISSN 0909-0495

Received 12 May 2008
Accepted 25 November 2008

High-flux hard X-ray microbeam using a single-bounce capillary with doubly focused undulator beam

Raul A. Barrea,[a]* Rong Huang,[b] Sterling Cornaby,[c,d] Donald H. Bilderback[c,d] and Thomas C. Irving[a]

[a]The Biophysics Collaborative Access Team (BioCAT), CSRRI and Department of Biological, Chemical and Physical Sciences, Illinois Institute of Technology, Chicago, IL 60616, USA, [b]IMCA-CAT, The Center for Advanced Radiation Sources, University of Chicago, Chicago, IL 60637, USA, [c]Cornell High Energy Synchrotron Source, Cornell University, Ithaca, NY 14853, USA, and [d]School of Applied and Engineering Physics, Cornell University, Ithaca, NY 14853, USA.
E-mail: rbarrea@gmail.com

A pre-focused X-ray beam at 12 keV and 9 keV has been used to illuminate a single-bounce capillary in order to generate a high-flux X-ray microbeam. The BioCAT undulator X-ray beamline 18ID at the Advanced Photon Source was used to generate the pre-focused beam containing 1.2×10^{13} photons s^{-1} using a sagittal-focusing double-crystal monochromator and a bimorph mirror. The capillary entrance was aligned with the focal point of the pre-focused beam in order to accept the full flux of the undulator beam. Two alignment configurations were tested: (i) where the center of the capillary was aligned with the pre-focused beam ('in-line') and (ii) where one side of the capillary was aligned with the beam ('off-line'). The latter arrangement delivered more flux (3.3×10^{12} photons s^{-1}) and smaller spot sizes (≤ 10 µm FWHM in both directions) for a photon flux density of 4.2×10^{10} photons s^{-1} μm^{-2}. The combination of the beamline main optics with a large-working-distance (approximately 24 mm) capillary used in this experiment makes it suitable for many microprobe fluorescence applications that require a micrometer-size X-ray beam and high flux density. These features are advantageous for biological samples, where typical metal concentrations are in the range of a few ng cm^{-2}. Micro-XANES experiments are also feasible using this combined optical arrangement.

Keywords: single-bounce capillary; microprobe; microbeam; microfluorescence; micro-XANES.

1. Introduction

Considerable effort has been dedicated over the last decade to developing focusing devices capable of delivering X-ray beams of micrometer and submicrometer size for a wide range of spectroscopic and diffraction applications ranging from materials science and environmental science to biomedical studies. These efforts have culminated in a variety of technical approaches, each with their own advantages and disadvantages for particular applications. Factors that need to be considered when selecting an optical scheme are the final focal spot size, degree of chromaticity, focal distance, flexibility to change focus size dynamically during an experiment, total beam flux and beam flux density among others.

Reflecting Kirkpatrick–Baez (KB) mirrors (Kirkpatrick & Baez, 1948; Ziegler *et al.*, 2004) are widely used as focusing devices; most of the efforts in their continuing development are dedicated to obtaining better quality mirrors to achieve submicrometer focal spots (Yamauchi *et al.*, 2007; Hignette *et al.*, 2007; Paterson *et al.*, 2007; Reininger & Dhesi, 2007). Their achromaticity allows the focal point to be maintained while the energy is tuned, an essential feature for spectroscopy experiments. Their typical delivered flux, $\sim 3 \times 10^{11}$ photons s^{-1}, at undulator beamlines can be increased by using multilayer monochromators, relaxing the energy resolution [$\Delta E/E \simeq 10^{-4}$ for a Si(111) crystal *versus* $\Delta E/E \simeq 10^{-2}$ for a multilayer crystal]. KB mirrors have been combined with sagittally bent crystals to increase the delivered flux from a bending-magnet beamline (Ziegler *et al.*, 2004) with a focal spot size of 2.6 µm [vertically (V)] × 6.8 µm [horizontally (H)] FWHM and irradiance gain of 2.6×10^4.

Alternative focusing devices include Fresnel zone plates (Baez, 1961; Snigireva *et al.*, 2007; Maser *et al.*, 2004) that use diffraction to deliver nanometer-size beams while maintaining

the incident beam coherence, an important feature for X-ray phase-contrast imaging. Current development efforts are driven by the desire to achieve very small beams of the order of a few nanometers (Chu *et al.*, 2008). The efficiency of the zone plates is about 40 to 50% and can provide a very high photon flux density that substantially improves the elemental detection limit. Typical delivered flux in the hard X-ray regime is $\sim 10^9$ photons s^{-1} at third-generation sources. Compound refractive lenses (Snigirev *et al.*, 1996; Snigirev, Snigireva *et al.*, 2007) closely approximate a true X-ray lens. They are compact, robust and easy to operate and they work best in the energy region 15–80 keV.

Capillaries have also been used for synchrotron microbeam experiments for many years. They may be classified into three different categories: polycapillaries (Kumakhov, 2000; Bjeoumikhov *et al.*, 2008), multi-bounce capillaries (Engström & Riekel, 1996) and single-bounce capillaries (Huang & Bilderback, 2006). These are achromatic devices, making them suitable for spectroscopy experiments. It has been a challenge to make capillaries of sufficiently high optical quality to match the very low emittance of a third-generation source. While there have been reports of applications of single-bounce capillaries at third-generation synchrotron facilities (Snigirev, Bjeoumikhov *et al.*, 2007), they are not yet widely used, especially for applications that require high-flux microbeams with moderate spatial resolution.

The BioCAT microprobe instrument on beamline 18ID of the Advanced Photon Source, Argonne National Laboratory, is dedicated to microfluorescence studies on biological samples (Barrea *et al.*, 2006). The purpose of these studies is to determine the distribution and chemical speciation of the elemental content on large tissue sections. The beam absorbed by a typical 10–20 μm-thick sample is very small and most of the incoming X-ray beam is transmitted. Under these conditions the throughput of the microprobe is limited by the X-ray beam flux delivered to the samples. The current optical configuration of the microprobe comprises an Xradia 100 mm-long pair of KB mirrors, which routinely provide 5 μm FWHM focal spots of 3.0×10^{11} photons s^{-1} at 12 keV. The mirrors' aperture, set by a pair of slits, is 0.4 mm (V) × 0.4 mm (H). Additionally, the ability to maintain a fixed focal point while scanning energies is essential for speciation measurements. These are time-consuming experiments and they are usually performed only on selected sample spots. Any strategy that increases the flux delivered would directly translate into reduced scan times and, hence, higher throughput. The delivered flux can be significantly increased either by increasing the beam acceptance of the optical device or by using a pre-focused incident beam. Taking into consideration the second option, we decided to explore the capabilities of a combined optical scheme. Considering that BioCAT's microprobe program is mainly devoted to micrometer-scale fluorescence mapping of tissue samples, such an optical configuration could satisfy the demands for high flux at a sufficiently small X-ray beam size for most applications with biological tissues with a modest investment of resources. This approach allowed us to optimize our optical configuration to a regime that has not been addresses by other optics.

Here we show that with appropriate pre-focusing a single-bounce capillary can be an effective focusing device for producing microbeams with high flux density. Single-bounce capillaries have the advantage of being able to provide large working distances with an X-ray throughput that is virtually independent of beam energy. This combination can yield useful microbeams (<10 μm FWHM) with 3×10^{12} photons s^{-1} at 12 keV and good stability during energy scans. This provides several advantages for mapping experiments. Firstly, it allows for speeding up the scanning process by reducing the acquisition time significantly, making mapping speciation experiments feasible for thin biological samples. Secondly, it also improves the sensitivity of the microprobe because of the higher flux density.

2. Experimental

APS undulator A provides a source of very intense monochromatic radiation over a wide range of X-ray energies: 3.2–42 keV (first and third harmonic). The typical source size is 11.0 μm (V) × 271.3 μm (H). The photon flux delivered by the unfocused beam at 12 keV is 1.18×10^{13} photons s^{-1} at 100 mA ring current and a beam size of 1 mm (V) × 2 mm (H) (50 m downstream of the source). A cryo-cooled Si(111) double-crystal monochromator, located 54 m downstream of the source, covers the energy range 3.4–14.6 keV using the fundamental of the undulator spectrum. The 18ID monochromator has a sagittal-focusing second-crystal assembly that provides for horizontal focusing of the beam. There is no loss of intensity when the beam is focused horizontally, and near-theoretical spot sizes are achieved. We have observed a horizontal intensity profile of 195 μm (221 μm) FWHM after sagittal focusing at 12.0 keV (9.0 keV) at the focal point (demagnification ratio of 3.1:1). A 600 mm-long bimorph mirror (56 m downstream of the source) is used for harmonic rejection and vertical focusing. A vertical intensity profile of 125 μm (100 μm) FWHM was measured at 12.0 keV (9.0 keV) at the focal point (demagnification ratio of 4:1). Downstream of the mirror are horizontal and vertical beam-defining slits for the monochromatic beam. Additional details of the beamline optics can be found elsewhere (Fischetti *et al.*, 2004).

The capillary used in this experiment was designed and made originally for the wiggler beam at the CHESS G-line, with a measured capillary tip-to-focus distance of 24 mm. The capillary length itself is 40 mm, with an entrance diameter of 310 μm and exit diameter of 196 μm. This capillary was designed to have a full divergence of 8.0 mrad that corresponds to a maximum reflection of about 2.0 mrad, and it should be able to work with X-ray energies up to 15 keV without losing its reflectivity. The quality of this capillary was first tested at the CHESS G-line (a multipole wiggler beamline), where the RMS source size is 1400 μm (H) × 360 μm (V). The X-rays from this source were vertically collimated with a mirror at 23 m from the source and horizontally focused with a sagittally curved multilayer at 28.5 m with its focal

position at 37 m from the source. A set of aperture slits were located at 30 m from the source to limit the horizontal acceptance to 1 mm. When this capillary distance was set at about 6.5 m from the sagittal multilayer, the focal spot of the capillary optic is scanned using a 5 μm pinhole. The focused spot size was 9.2 μm (H) × 10.8 μm (V) FWHM [10.5 μm (H) × 11.9 μm (V) before deconvolution of the 5 μm pinhole], a size suitable for most of the microspectroscopy experiments at the BioCAT facility. The capillary reflectivity was about 95%.

The capillary was not optimized for undulator radiation at the APS. At 18ID the incident beam is pre-focused both vertically and horizontally, so that the convergence of the incident X-rays to the capillary will be similar to that at the CHESS G-line. With the APS undulator source horizontal divergence of 11.4 μrad RMS, the horizontal FWHM divergence after sagittal focusing will be about 90 μrad, similar to the slope errors of the capillary used (Huang & Bilderback, 2006). Three-dimensional ray-tracing calculations using the Monte Carlo method showed that the focal spot size and working distance should be the same as that measured at the CHESS G-line, 10 μm and 24 mm, respectively.

Another concern was that there is a significant amount of flux lost through the capillary tip opening, which is 196 μm in diameter, comparable with the incident beam size. This could, in principle, be reduced if only one side of the capillary is used. Normally, when the capillary is illuminated fully with X-rays, an X-ray ring that is concentric with the direct X-ray spot can be viewed as a far-field fluorescence image (Bilderback & Huang, 2001) and this concentricity has been used for capillary alignment. When the capillary is not fully illuminated there is only an arc instead of a ring that is used for capillary alignment. This situation was also studied by three-dimensional ray tracing (see Figs. 1 and 2). The numerical results showed that, once the capillary is aligned with full illumination at BioCAT, its focusing quality will not be changed when vertically translated; only the focal position will be moved vertically by the same distance. Therefore, during the experiment, we followed this alignment procedure suggested from the numerical simulation.

The capillary was mounted on a holder consisting of an aluminium plate with a V groove shape. The holder was covered with an acrylic cap and it was kept under a constant He flow during the X-ray exposure in order to minimize radiation damage. The holder was mounted on an XY positioner including rotary and tilt stages, which provide all the necessary degrees of freedom for alignment of the capillary. The entrance aperture of the capillary is located at the center of rotation of the rotary stage and tilt stage for easy alignment. A beam stop was made by slicing a very small section of a 210 μm-diameter tungsten rod. It was positioned slightly upstream and close to the capillary entrance. The beam-stop holder was mounted on an independent XY positioner that allows movement relative to the capillary entrance for alignment purposes (Falkenberg *et al.*, 2003). The diameter of the beam stop was chosen to be slightly larger than the capillary tip opening because of some irregularity of the rod after slicing and also because of the divergence of incident X-rays to the capillary. This allowed the beam stop to completely block the incoming beam that passed through the capillary exit aperture.

An ion chamber and a set of collimator slits upstream of the capillary holder were used as the beam monitor and beam-defining slits, respectively. Downstream of the capillary tip was

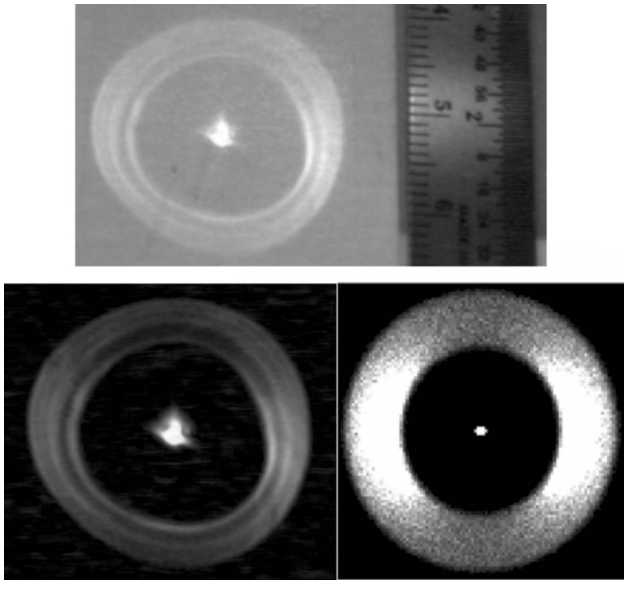

Figure 1
Top: far-field image without beam stop; the ruler shows the actual size of the image (approximately 25 mm outer diameter). Bottom: the same rings with external lights turned off for better contrast, and its ray-tracing simulation.

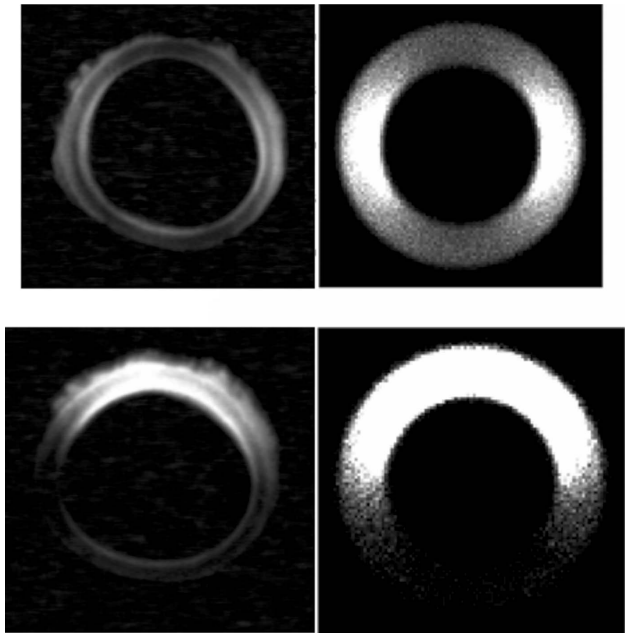

Figure 2
Far-field images with beam stop in place with the direct beam completely blocked. The top images show the capillary aligned 'in-line' with the main beam, and its ray-tracing simulation. The bottom images show the capillary aligned 'off-line' with the main beam, and its corresponding ray-tracing simulation. The irregularities of the image of the outer rings are due to the irregular shape of the beam stop.

an XYZ stage that supported the sample holder oriented at 45° relative to the direction of the incident beam. A second ion chamber was located downstream of the sample holder to monitor the micrometer-size beam when there is no sample in the beam path. A Si pin diode was also used as an intensity monitor when there are samples mounted on the XYZ stage. This pin diode was mounted on top of the capillary holder to measure the scattered beam by the air path near the capillary tip. A video camera with large working distance was aligned normal to the sample surface at 45° to the incoming beam direction. The camera was used as a reference point in fluorescence measurements, allowing the alignment of the samples at the X-ray focal spot. A Ketek 100 mm^2 active-area silicon drift detector (SDD) with XIA Saturn electronics completed the experimental arrangement.

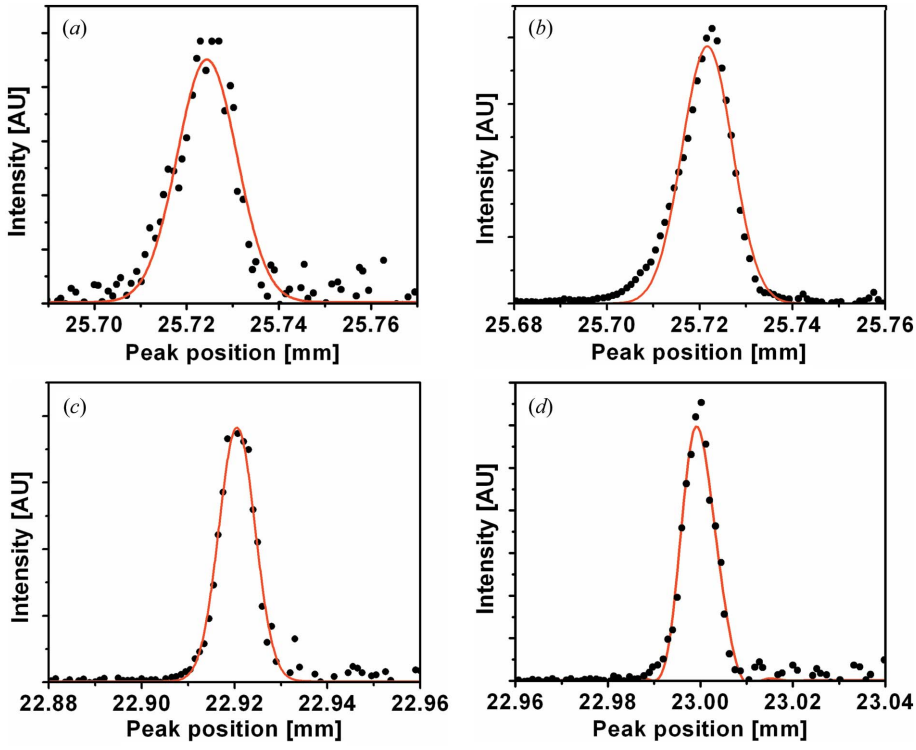

Figure 3
Horizontal beam profiles at 12 keV: (*a*) capillary in-line (12.3 µm FWHM); (*b*) capillary off-line (10.1 µm FWHM). Vertical beam profiles at 12 keV: (*c*) capillary in-line (10.1 µm FWHM); (*d*) capillary off-line (9.2 µm FWHM).

2.1. Far-field images of the beam

Far-field images were obtained by placing a fluorescence screen downstream of the capillary at 5 m from the capillary tip. Far-field images are very convenient for optimizing the alignment of the capillary with the pre-focused beam and the alignment of the beam stop to prevent radiation leakage. Alternative approaches, such as measuring the beam flux at the focal spot, did not allow us to detect small radiation leaks owing to a misaligned beam stop. We also used these far-field images to monitor the stability of the combined optics configuration, since any changes of the alignment will be reflected and magnified on these images. The projection of the microbeam on the fluorescence screen shows an outer diameter of about 2.5 cm (Fig. 1). We did not observe any shifts or changes of the images during the course of the experiment, indicating very good stability of the combined optical configuration. The far-field images were captured by a CCD video camera and recorded to further analyze the different configurations of the capillary alignment, beam stop alignment and beam stability during energy scans.

Alignment of the capillary was achieved by moving the tilt and rotary stages while observing both the transmitted intensity and the far-field images. When the capillary is properly aligned, the rings in the far-field image are concentric to the direct beam. Fig. 1 shows the far-field images with the capillary aligned 'in-line' with the beam with and without the beam stop. When the capillary is misaligned, the rings are not circular and the direct beam is not centered. The downstream ion chamber also allows determination of the proper alignment of the capillary by maximizing the delivered X-ray intensity.

Beam-stop alignment was performed by moving the XY positioner relative to the capillary position. The direct beam was then blocked as well as part of the otherwise reflected beam, because of the irregular shape of the beam stop. Outer rings represent the beam reflected near the tip. Fig. 2 shows the far-field images when the capillary is aligned 'off line' with the pre-focused incoming beam. The image is inverted, thus the top part of the image corresponds to the bottom part of the capillary. The effect of the beam-stop shape is clearly observed. The tail of the pre-focused beam illuminates the other side of the capillary causing a low intensity contribution on the lower part of the image. This contribution can be removed by closing the upstream beam-defining slits on the corresponding side, with the effect of decreased flux intensity.

During the experiment we tested a number of different alignment conditions. Firstly, we moved the capillary horizontally or vertically by small amounts (∼15 µm steps in either directions) to illuminate different regions of the capillary walls. This procedure required relocation of the beam-stop position as well. Under these conditions the beam projection on the far-field screen moved accordingly. This simple test allowed us to observe the effect of a parallel shift of the direct beam. As the direct beam illuminated different regions of the capillary walls, the reflected beam intensity slightly changed but no changes in the circular shape of the rings were observed. The horizontal focus position (see Fig. 3) did not change when the beam was displaced vertically to illuminate only one side of the capillary. The vertical focus position shifted 80 µm reflecting the 80 µm displacement of

Table 1
Beam intensities measured with an ion chamber located 23 cm downstream of the capillary.

Values were corrected for air absorption.

	Intensity ($\times 10^{12}$ photons s^{-1})					
		Capillary in-line		Capillary off-line – Top section		Capillary off-line Bottom section
Energy	Direct beam No Capillary	No beam stop	With beam stop	No beam stop	With beam stop	With beam stop
12 keV	10.6	7.99	1.77	6.78	2.95	3.09
9 keV	7.88	6.05	1.50	7.29	2.84	3.30

the capillary–beam-stop system required to obtain the off-line alignment condition. This clearly shows that either vertical or horizontal parallel shifts of the beam would not change the focal position.

During the alignment process we also changed the rotation and tilt of the capillary. The immediate result in both cases (moving the rotation or tilt positions) is the distortion of the shape of the rings from circular to oval shape. Direct beam leakage was also observed because the beam stop was not properly aligned. Each new capillary position required the relocation of the beam stop to block the direct beam. As mentioned before, measuring the beam intensity alone was not sufficient to detect these small changes. Since the capillary focuses the X-ray beam at a very short focal distance ($\sim$24 mm), a 10 µm motion at the capillary focal position could only be caused by a direct beam shift of 5–10 mm at the monochromator position (about 20 m upstream of the capillary) should the upstream beam move. This extreme shift would immediately be accounted for by the beam-defining collimator slits. These tests allowed us to evaluate the sensitivity of the far-field image to detect small angular variations of the optical configuration. When scanning the direct beam to perform XANES measurements, the capillary beam-stop system remained aligned with the beam. No leakage or distortion of the ring shape was observed during the experiment.

2.2. Beam intensity

The delivered flux was firstly measured without the capillary in the beam path, using an ion chamber located downstream of the capillary holder. This value was used later as the reference intensity for determination of the system's efficiency: pre-focused beam, upstream slits, capillary and beam stop. Microbeam intensities were measured in both configurations, (i) in-line and (ii) off-line, using the same ion chamber. Table 1 shows the results obtained at 12 keV and 9 keV excitation energies. Although the undulator beam intensity was 1.18×10^{13} photons s^{-1}, the capillary's incoming intensity was slightly reduced by the fact that the pre-focused beam was larger than the capillary entrance aperture. Part of the incoming beam is blocked by the beam-defining slits located upstream of the capillary. Another part of the incident beam, which would otherwise be reflected by the capillary, is also blocked by the beam stop because of its irregular shape.

When the capillary was aligned in configuration (i) (in-line) approximately 76% of the incoming beam is transmitted, including the reflected and direct beam at either 12 keV or 9 keV. The effect of the beam stop on the delivered flux was significant in this configuration, where overall throughput of the set-up was just 22–25% of the incoming beam.

In an attempt to maximize the delivered flux in the focused beam we investigated configuration (ii) (off-line), where the capillary was aligned off-center with the pre-focused beam. We found that under this configuration the reflected intensity increased by almost two times for an overall throughput of about 38–54%. As can be seen from Table 1, either the top or bottom sections of the capillary delivered equivalent X-ray flux.

2.3. Beam profiles

The capillary nominal focal distance was 24 mm. We used a $CdWO_4$ crystal as a fluorescence screen, placed at the capillary focal position to visualize the beam shape and to find the correct position for our knife-edge scans. A silicon wafer coated with a thin Ni film was used as the knife edge. The Ni $K\alpha$ fluorescence emission was measured using an SDD located at 90° to the direction of the main beam. Knife-edge scans were performed at 12 keV and 9 keV in both vertical and horizontal directions, in both in-line and off-line configurations. We observed a smaller beam profile when the capillary was aligned off-line. Fig. 3 shows the beam profiles at 12 keV in both configurations. Similar results were obtained at 9.0 keV.

2.4. Energy and fluorescence mapping scans

Another characteristic of this optical system is its capacity to maintain the focal spot at a fixed position while scanning the energy for spectroscopy experiments. The energy dependence of the focal spot has been previously measured in the energy range 7–40 keV (Falkenberg *et al.*, 2003). The capillary was aligned with the pre-focused beam at 9.0 keV, and the monochromator's energy was scanned over a 400 eV range around the Cu *K*-edge. We followed the far-field image during the energy scans to observe the beam position stability. The far-field rings did not show any drift or shift in position, evidencing a highly stable focus position. Thus, this configuration is suitable for XANES experiments. Fig. 4 shows XANES spectra of a Cu foil (measured in transmission mode)

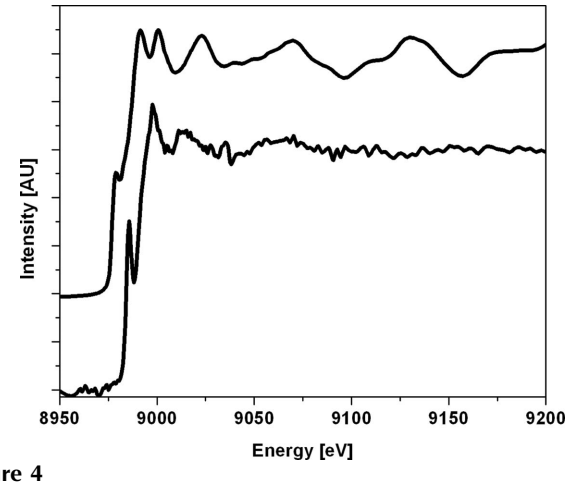

Figure 4
XANES spectra of a Cu foil (used as reference) (top) and a NIST standard (oyster tissue, NIST #1566b) (bottom), measured in transmission mode and in fluorescence mode, respectively. The microbeam position was monitored by following the far-field image during the energy scan. No change in beam position was observed during the scans.

and a NIST standard oyster tissue sample #1566b measured in fluorescence mode.

Finally, we performed fluorescence mapping scans using the capillary configuration and compared them with those taken with the existing KB mirror system (Xradia, with 100 mm-long mirrors and a 0.4 mm acceptance for the incoming unfocused parallel undulator beam). The samples were 10 µm-thick mouse prostate tissue sections, mounted on an 8 µm-thick Kapton film, supported by a clear acrylic frame. A more detailed description of the samples and the animal experiment can be found elsewhere (Barrea *et al.*, 2009). With the high-flux capillary microbeam, we observed a strong saturation of our SDD detector. To avoid saturation, we attenuated the incoming beam by ∼3.8-fold using Al filters for this particular measurement. Thinner samples or those with low metal abundance did not require attenuation. The acquisition time per pixel for the capillary set-up was 0.5 s per pixel (with 3.8 times attenuation) and the acquisition time for the KB mirror set-up was 1.0 s per point (no attenuation). (Including the beam attenuation factor, the actual reduction in acquisition time could be, therefore, 7.6-fold.) A typical scan, with an average of 10000 pixels per sample, requires 2.7 h with KB mirrors and only 1.3 h with the capillary. This allows us to scan more samples in the same time frame with similar data quality. A set of elemental maps of normal and tumor prostate tissue, measured using the capillary optics, is shown in Fig. 5. The images show the distribution of different metals (Fe, Cu and Zn) in the samples. The quality of the images is clearly seen. The count rate per pixel with the capillary configuration is about eight times the count rate using KB mirrors.

3. Discussion and conclusions

We have described an optical system where the main beamline focusing optics are combined with a single-bounce capillary that is capable of delivering 10 µm-size X-ray beams with very high flux (∼3.1 × 10^{12} photons s^{-1} at 12.0 keV and 9.0 keV, about 30% of the total undulator flux). With this focusing set-up, the gain of X-ray flux in the focal spot over the unfocused beam is of the order of 10^4. Further improvements, however, are possible.

The flux delivered by this set-up is limited by the pre-focused beam profile, the capillary acceptance diameter and the size and uniformity of the beam stop. We expect to be able to reduce the vertical pre-focused beam size down to 40 µm FWHM with upgrades to the bimorph mirror system. This

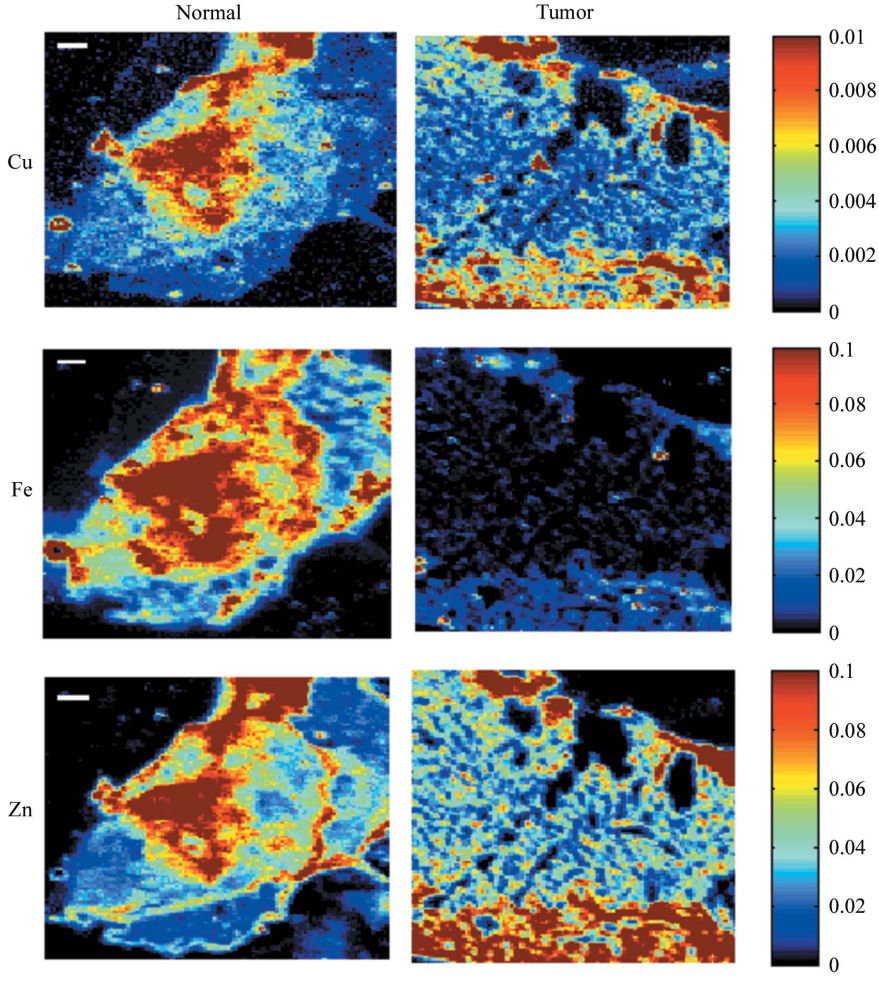

Figure 5
Cu, Fe and Zn content of normal and tumor prostate tissue. Color scale units are µg cm^{-2}; size scale: 100 µm. Samples courtesy of Dr Ping Dou and Dr Di Chen at Karmanos Cancer Institute, Wayne State University, USA.

upgrade is in progress. Sagittal focusing, on the other hand, is already fully optimized. Another source of intensity loss is the irregular shape of the beam stop. A proper sized beam stop with a more regular shape will minimize the beam loss near the tip of the capillary. We expect to increase the delivered flux by at least twofold after implementing these upgrades.

Two other factors limit the performance of the microprobe: the maximum count rate of the SDD and the overhead time of the step scan mode. The need for high-count-rate energy-dispersive detectors is very well known. As mentioned before, most of the microfocusing devices currently in use deliver beam fluxes in the 10^9–10^{11} photons s^{-1} range. Under these conditions, solid state detectors can handle the fluorescence yields depending on the sample composition. As was observed, X-ray beams of 10^{12}–10^{13} photons s^{-1} can easily saturate the detection system with the consequent non-linear distortions of the spectrum and the requirement for large dead-time corrections. Bent Laue crystal analyzers (BCLAs) are an attractive alternative for these detection systems (Kropf *et al.*, 2003). Since these are wavelength-dispersive systems, they are not suitable for microprobe elemental fluorescence scans but can be very useful for XAFS spectroscopy measurements. We are planning to implement these BCLA analyzers combined with continuous scan mode for speciation mapping applications. Although continuous scan modes (Barrea *et al.*, 2006) are available for two-dimensional scans at the BioCAT beamline, they were not used for the experiments reported here because they currently do not store the full spectrum from the SDD detector. Upgrades to provide this capability are under development.

It can also be seen from Fig. 1 that the present far-field capillary rings are not smooth and round, a clear indication of the existence of capillary figure errors which are simulated as slope errors in our ray-tracing. To give us an idea of to what extent the capillary slope errors affected our focusing, a ray-tracing simulation for our optical arrangement, with the same pre-focusing optics design but now for a perfect capillary, was performed and it predicted a focal spot size of 3 μm FWHM. Thus if we could reduce the capillary slope errors (which are currently about 0.1 mrad) to half this value, we should be able to produce a tighter focal size (∼4–5 μm) with a capillary of the same design. For most of our biological applications there is no need for X-ray energies higher than 12 keV, which means the maximum total reflection angle can be as large as 3.3 mrad for a glass capillary. A 'fatter' capillary can be designed specifically for our beamline optics with X-ray total divergence after capillary focusing as large as 13 mrad. There is clearly room to improve the focusing capabilities of this system if higher quality capillaries can be fabricated.

In summary, using long-working-distance tapered capillaries with pre-focusing optics can provide a high-flux microbeam that can help make practical high-throughput microfluorescence and microspectroscopy applications on biological samples with moderate spatial resolution.

Use of the Advanced Photon Source was supported by the US Department of Energy, Basic Energy Science, Office of Energy Research, under Contract No. W-31-109-Eng-38. BioCAT is a NIH-supported Research Center, RR08630. The content is solely the responsibility of the authors and does not necessarily reflect the official views of the National Center for Research Resources or the National Institutes of Health. The CHESS work is supported by the National Science Foundation and NIH-NIGMS *via* NSF grant DMR-0225180. Dr Q. Ping Dou and Dr Di Chen (Karmanos Cancer Institute, Wayne State University, Detroit, MI, USA) are gratefully acknowledged for kindly providing the tissue samples.

References

Baez, A. (1961). *J. Opt. Soc. Am.* **51**, 405–412.
Barrea, R. A., Chen, D. & Dou, P. (2009). In preparation.
Barrea, R. A., Gore, D., Kondrashkina, E., Weng, T., Heurich, R., Vukonich, M., Orgel, J., Davidson, M., Collingwood, J. F., Mikhaylova, A. & Irving, T. C. (2006). *Proceedings of the 8th International Conference on X-ray Microscopy (XRM2005), IPAP Conference Series 7*, Himeji, Japan, 26–30 July 2005, pp. 230–232.
Bilderback, D. & Huang, R. (2001). *Nucl. Instrum. Methods Phys. Res. A*, **467**, 970–973.
Bjeoumikhov, A., Erko, M., Bjeoumikhova, S., Erko, A., Snigireva, I., Snigirev, A., Wolff, T., Mantouvalou, I., Malzer, W. & Kanngiesser, B. (2008). *Nucl. Instrum. Methods Phys. Res. A*, **587**, 458–463.
Chu, Y. S. *et al.* (2008). *Appl. Phys. Lett.* **92**, 103119.
Engström, P. & Riekel, C. (1996). *J. Synchrotron Rad.* **3**, 97–100.
Falkenberg, G., Rickers, K., Bilderback, D. H. & Huang, R. (2003). In *HASYLAB 2003 Annual Report.* HASYLAB, Hamburg Germany.
Fischetti, R., Stepanov, S., Rosenbaum, G., Barrea, R., Black, E., Gore, D., Heurich, R., Kondrashkina, E., Kropf, A. J., Wang, S., Zhang, K., Irving, T. C. & Bunker, G. B. (2004). *J. Synchrotron Rad.* **11**, 399–405.
Hignette, O., Cloetens, P., Morawe, C., Borel, C., Ludwig, W., Bernard, P., Rommeveaux, A. & Bohic, S. (2007). *AIP Conf. Proc.* **879**, 792–795.
Huang, R. & Bilderback, D. H. (2006). *J. Synchrotron Rad.* **13**, 74–84.
Kirkpatrick, P. & Baez, A. (1948). *J. Opt. Soc. Am.* **38**, 766–773.
Kropf, A. J., Finch, R. J., Fortner, J. A., Aase, S., Karanfil, C., Segre, C. U., Terry, J., Bunker, G. & Chapman, L. D. (2003). *Rev. Sci. Instrum.* **74**, 4696–4702.
Kumakhov, M. A. (2000). *X-ray Spectrom.* **29**, 343–348.
Maser, J., Stephenson, G. B., Shu, D., Lai, B., Vogt, S., Khounsary, A., Li, Y., Benson, C. & Schneider, G. (2004). *AIP Conf. Proc.* **708**, 470–473.
Paterson, D. J., Boldeman, J. W., Cohen, D. D. & Ryan, C. G. (2007). *AIP Conf. Proc.* **879**, 864–867.
Reininger, R. & Dhesi, S. (2007). *AIP Conf. Proc.* **879**, 567–570.
Snigirev, A., Bjeoumikhov, A., Erko, A., Snigireva, I., Grigoriev, M., Yunkin, V., Erko, M. & Bjeoumikhova, S. (2007). *J. Synchrotron Rad.* **14**, 227–228.
Snigirev, A., Kohn, V., Snigireva, I. & Lengeler, B. (1996). *Nature (London)*, **384**, 49–51.
Snigirev, A., Snigireva, I., Grigoriev, M., Yunkin, V., Di Michiel, M., Kuznetsov, S. & Vaughan, G. (2007). *Proc. SPIE*, **6705**, 670506.
Snigireva, I., Snigirev, A., Kohn, V., Yunkin, V., Grigoriev, M., Kuznetsov, S., Vaughan, G. & Di Michiel, M. (2007). *Proc. SPIE*, **6705**, 67050G.
Yamauchi, K., Mimura, H., Matsuyama, S., Yumoto, H., Handa, S., Yamamura, K., Sano, Y., Endo, K., Mori, Y., Nishino, Y., Tamasaku, K., Yabashi, M. & Ishikawa, T. (2007). *AIP Conf. Proc.* **879**, 786–791.
Ziegler, E., Bigault, T. & Hoszowska, J. (2004). *AIP Conf. Proc.* **705**, 768–771.